Abdel-Malek, K., 1995,"Dexterity of Manipulator Arms at an Operating Point," ***Proceedings of the 21st ASME Advances in Design Automation*****, DE Vol. 82(1), pp. 781-788.**

DEXTERITY OF MANIPULATOR ARMS AT AN OPERATING POINT

Karim Abdelmalek
Department of Mechanical Engineering and
Center for Computer Aided Design
The University of Iowa
Iowa City, IA 52242

ABSTRACT

This paper presents a method for analyzing dexterity, hence functionality of robotic manipulators at an operating point. Dexterity of Manipulators comprising spherical wrists is studied. The goal is to provide the user with knowledge of orientability of the end-effector at a target. Wrist accessible output sets are determined analytically by first determining manipulator singularities, followed by back substituting the singularities into the constraint equations to parametrize surfaces. Since regions of a surface may exist inside the wrist accessible output set, and other regions on the boundary, surfaces are segmented into subsurfaces. The segmentation of surfaces is carried out using intersection methods to compute higher order singularities. To determine whether a subsurface is an internal or boundary one, each subsurface is studied for existence inside the wrist accessible output set by perturbing a point along its normal. Closed-form solutions of the boundary of the wrist accessible output set are obtained.

A service sphere is located at an operating point in the accessible output set and the sphere is intersected with the boundary sub-surfaces. The intersection curves are computed and projected onto the space of a cylinder, then the cylinder is unrolled to depict a map. Dexterity charts are introduced as maps depicting orientability of the end-effector at a target. The problem of service region overlapping is solved by projecting the solutions onto dexterity charts and superimposing service regions.

1 INTRODUCTION

This paper is aimed at obtaining an improved understanding of the functionality of robotic arms. In the past, researchers in the field of robotics have studied functionality in terms of spaces. Reachable workspaces have been addressed by Roth (1975), Tsai and Soni (1981), Yang and Lee (1983), Gosselin (1990), Emiris (1993), and Haug et al. (1994). Dexterous workspaces have been studied by Kumar and Waldron (1980), Yang and Lai (1985), and Wang and Wu (1993). Workspaces, however, do not provide adequate information about the functionality of the robot at specific targets. For example, given a required dexterous workspace using the current methods, one cannot determine a suitable placement of the robotic arm to attain maximum functionality.

The health care system is a key area in which a better understanding of functionality will have great impact. In brain surgery, for example, a surgeon may require the end-effector of a manipulator carrying a laser for tissue destruction to be positioned in several different orientations near a malignant tumor (Lavallee 1991). Thus, a knowledge of possible orientations of the end-effector at the target is of great importance to the surgeon. A measure of the “amount of dexterity”, called the Dexterous Solid Angle (DSA), was analytically defined by Abdel-Malek and Paul (1994).

Spine surgery is another example in which knowledge of the DSA is needed. This type of surgery is one of the more complicated procedures performed by surgeons. In particular, a robot can assist surgeons in inserting pedicle screws during spinal fusion to correct scoliosis. Determination of the DSA at each screw location will provide the surgeon with improved flexibility in manipulation.

In preparing a cavity for a prosthesis, a robot arm must follow the contour of a pre-planned trajectory defined by the prosthesis geometry. To obtain maximum functionality, the robot operator makes the choice of the location of the robot base. With the aid of "dexterity charts", exhibiting the functionality at specific targets, the robot operator will be able to better make this decision.

In an assembly cell on the shop floor of a manufacturing environment, a manipulator is needed to assemble a product in one cell while performing another task in another cell. The questions of where to locate the two cells with respect to the robot for maximum functionality may arise. To set the background for this paper, definitions of relevant terms are stated.

Accessible Output Set (Haug et al. 1994) The region of space that can be reached by a point on the manipulator, for all combinations of joint coordinates.

Dexterous Workspace (Kumar and Waldron, 1981) A subspace of the accessible output set within which a vector on the end-effector may assume all orientations. Because of joint limits and geometric constraints (e.g., at workspace boundaries), the dexterous workspace may not include all of the accessible output set.

Wrist Point When a manipulator hand (end effector) may be modeled as a rigid body that rotates about a point **W** fixed in some link of the manipulator, **W** is referred to as the **wrist point**. Most often, W will be located at the intersection of three successive revolute joints, in a chain of three links.

Wrist Accessible Output Set: The set of points that can be accessed by the wrist point.

Service Sphere: A sphere parametrized as $\mathbf{x}_{ss}(\mathbf{p})$ centered at **p** that is used to indicate dexterity at an operating point **p**. The service sphere can assume any radius less than the length of the last link of the manipulator. The terms "Service Sphere" and "Service Angle" were first introduced by Vinagradov et al. (1971).

Service Point: Point on the service sphere through which the end-effector may penetrate.

Service Region: A Region $SR_i(\mathbf{p},\mathbf{q})$ on the service sphere containing only service points, where **q** is the vector of generalized coordinates. Note that there may be any number N_R of service regions, each of area $A_i(\mathbf{p})$. The total **service area** is therefore $\bigcup_{i=1}^{N_R} A_i(\mathbf{p})$.

Dexterous Solid Angle DSA(**p**) (Abdel-Malek and Paul 1994) The ratio of the total area of the service regions to the area of the service sphere at point **p**, i.e.,

$$DSA(\mathbf{p}) = \bigcup_{i=1}^{N_R} A_i(\mathbf{p}) \Big/ 4\pi h^2 \tag{1}$$

where *h* is the radius of the service sphere. Because DSA is not an angle in the ordinary sense, and because it is similar to the solid angle

$$\omega = \bigcup_{i=1}^{N_R} A_i(\mathbf{p}) \Big/ h^2 \tag{2}$$

it was called the Dexterous Solid Angle (DSA) which represents a measure of dexterity at an operating point. Open chain mechanisms such as robotic manipulators comprise a number of links connected via joints; e.g. prismatic, revolute, and spherical. Generalized coordinates $\mathbf{q}^* = [q_1, q_2, ..., q_m]^T \in R^n$, where *m* is the number of degrees of freedom, are used to characterize the configuration (position and orientation) of each link in the manipulator. A six degree-of-freedom arm with a spherical wrist can be thought of as having two segments. The first segment (first three joints) is responsible for positioning the wrist point ***W***. The second segment (spherical wrist) is responsible for the orientation of the end-effector.

2. BOUNDARY PARAMETRIZATION OF THE WRIST ACCESSIBLE OUTPUT SET

The combination of the first three joints, coupled with joint limits and internal singularities of the mechanism, may result in a complex accessible output set. In order to analytically find expressions for the boundary surfaces of this set, it is necessary (1) to develop a set of analytical criteria to obtain the positioning of the wrist in terms of the generalized coordinates, (2) determine the boundary surfaces due to singularities associated with the set, and (3) determine the subset of these surfaces due to joint limits.

The mathematics of positioning of the wrist point are readily available by the use of the Denavit-Hartenberg (D-H) representation (Denavit and Hartenberg 1955). The D-H representation provides a systematic method for describing the relationship between adjacent links. The 4×4 transformation matrix describing a transformation from link (i-1) to link i for a revolute joint is

$$ {}^{i-1}\mathbf{A}_i = \begin{bmatrix} \cos\theta_i & -\cos\alpha_i \sin\theta_i & \sin\alpha_i \sin\theta_i & a_i \cos\theta_i \\ \sin\theta_i & \cos\alpha_i \cos\theta_i & -\sin\alpha_i \cos\theta_i & a_1 \sin\theta_i \\ 0 & \sin\alpha_i & \cos\alpha_i & d_i \\ 0 & 0 & 0 & 1 \end{bmatrix} \tag{3} $$

where θ_i, depicted in Fig. 1, is the joint angle from $\mathbf{x}_{i-1}$ to the $\mathbf{x}_i$ axis, d_i is the distance from the origin of the (i-1)th coordinate frame to the intersection of the $\mathbf{z}_{i-1}$ axis with the $\mathbf{x}_i$, a_i is the offset distance from the intersection of the $\mathbf{z}_{i-1}$ axis with the $\mathbf{x}_i$ axis, and α_i is the offset angle from the $\mathbf{z}_{i-1}$ axis to the $\mathbf{z}_i$ axis.

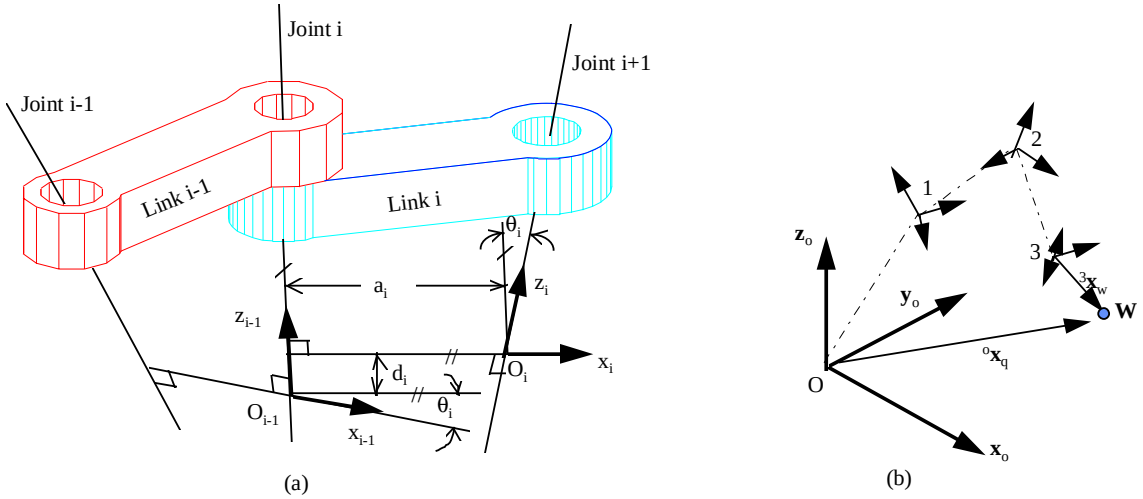

Figure 1 (a) DH Representation, (b) Notation used in obtaining the accessible output set

The homogeneous transformation matrix ${}^0\mathbf{T}_i$ that specifies the configuration of the ith frame with respect to the base coordinate system is the product of successive transformation matrices of ${}^{i-1}\mathbf{T}_i$,

$$ {}^0\mathbf{T}_i = {}^0\mathbf{T}_1\,{}^1\mathbf{T}_2 \ldots {}^{i-1}\mathbf{T}_i = \prod_{j=1}^{i} {}^{j-1}\mathbf{T}_j \tag{4} $$

where i is the number of degrees-of-freedom and ${}^{i-1}\mathbf{T}_i$ is of the form

$$ {}^{i-1}\mathbf{T}_i = \begin{bmatrix} {}^{i-1}\mathbf{R}_i & {}^{i-1}\mathbf{p}_i \\ 000 & 1 \end{bmatrix} \tag{5} $$

Where ${}^{i-1}\mathbf{R}_i$ is the rotation matrix between frame i-1 and frame i and ${}^{i-1}\mathbf{p}_i$ is the position vector from the origin of the i-1 frame to the ith frame. For a six axis manipulator with a spherical wrist, the homogeneous transformation matrix relating the end-effector and the wrist to the reference frame is

$$ {}^0\mathbf{T}_6 = {}^0\mathbf{T}_3\,{}^3\mathbf{T}_6 \tag{6} $$

The vector ${}^o\mathbf{x}_q$ describes the accessible output set of the wrist point such that

$$ {}^0\mathbf{x}_q = {}^0\mathbf{R}_3\,{}^3\mathbf{x}_w + {}^0\mathbf{p}_3 \tag{7} $$

where ${}^3\mathbf{x}_w$ is the vector describing the wrist point (Fig. 1b), resolved in the reference frame of link 3. In order to determine the boundary of the accessible output set for a mechanism, McKerrow (1991) showed that singularities (both internal and boundary) can be computed by proper manipulation of the Jacobian of the mechanism. Haug at al. (1994) presented a numerical method for mapping boundaries of accessible output sets for a general, multi degree-of-freedom mechanism. In this paper, first and higher order singularities are computed. Singularities are substituted into the constraint equation to parametrize boundaries of the *wrist* accessible output set.

For a given configuration of the manipulator, the generalized coordinates satisfy independent holonomic kinematic constraint equations of the form

$$ \Phi(\mathbf{q}) = {}^0\mathbf{x}_q - {}^0\mathbf{R}_3\,{}^3\mathbf{x}_w - {}^0\mathbf{p}_3 = 0 \tag{8} $$

Where $\Phi: R^n \rightarrow R^l$ is a smooth function, and l is the number of constraint equations. In addition, the generalized coordinates $\mathbf{q}$ are subject to inequality constraints representing joint limits.

$$ q_1^{\min} \le q_1 \le q_1^{\max} \tag{9a} $$

$$ q_2^{\min} \le q_2 \le q_2^{\max} \tag{9b} $$

$$ q_3^{\min} \le q_3 \le q_3^{\max} \tag{9c} $$

The constraint Jacobian of the constraint function $\Phi(\mathbf{q})$ of Eq. (8) for a certain configuration $\mathbf{q}^0$ is the 3×3 matrix

$$ \Phi_q(\mathbf{q}^0) = \left[\frac{\partial \Phi_i}{\partial q_j}\left(\mathbf{q}^0\right) \right] \tag{10} $$

The wrist accessible output set is thus

$$ A = \left\{ {}^0\mathbf{x}_q \in R^n \colon \Phi(\mathbf{q}) = \mathbf{0}, \quad \text{for some } \mathbf{q} \right\} \tag{11} $$

The boundary of the wrist accessible output set for a manipulator is a subset of the accessible output set at which the sub-Jacobian Φ_q of the kinematic constraint function of Eq. (8) is row-rank deficient (Haug et al. 1994), i.e.,

$$ \partial A \subset \left\{ {}^o\mathbf{x}_q \in A \colon \operatorname{Rank}\Phi_q(\mathbf{q}) < l, \text{ for some } \mathbf{q} \right\} \tag{12} $$

For a three degree-of-freedom mechanism (wrist accessible output set), equating the determinant of the Jacobian to zero will result in the singularities of the system. It is important to realize that some of these singularities will not satisfy the inequality constraints of the joint variables $\mathbf{q}$. To impose the inequality constraints, it is convenient to parametrize Eq. (9) by introducing new generalized coordinates λ_i such that for an inequality constraint of the form

$$ q_i^{\min} \le q_i \le q_i^{\max} \tag{13a} $$

can be parametrized as

$$ q_i = a_i + b_i \sin\lambda_i \tag{13b} $$

where $a_i = \left(q_i^{\max} + q_i^{\min}\right)/2$ and $b_i = \left(q_i^{\max} - q_i^{\min}\right)/2$ are the mid point and half range of the inequality constraint. The Jacobian with respect to the new coordinates can be written as

$$ \frac{\partial \Phi_i}{\partial q_j}\frac{\partial \mathbf{q}_j}{d\lambda_j} = \Phi_q \mathbf{q}_\lambda \tag{14a} $$

Singularities can be determined by equating the determinant of the Jacobian to zero such that

$$\mathbf{F}(\mathbf{x}) = \left|\Phi_q \mathbf{q}_\lambda\right| = 0 \tag{14b}$$

Solving $\mathbf{F}(\mathbf{x})$ and substituting the results into Eq. (13b), a set of first order singularities μ_i *(i=1,...,m)* is generated, where *m* is the total number of singularities. First order singularities generated by Eq. (14b) are of two types. *Internal* singularities are those due to the assembly of the mechanism itself. *Boundary* singularities are due to inequality constraints imposed on joints (e.g., space limitation, interference, and actuator capability).

Equation 14b is used to find the boundary of the wrist accessible output set in closed form. It is of interest to parametrize the boundary of the wrist accessible output set to later compute the intersections of the boundaries with the service sphere to determine service regions. Solutions are then projected onto another space to visualize the service regions.

Substituting each singularity into the accessible output set Eq. (7), a set of surfaces $\mathrm{X}^\iota(\mu_\iota)$ are parametrized such that

$$\mathrm{X}^i(\mu_\iota) = \left[\mathbf{x}^1(\mu_1), \mathbf{x}^2(\mu_2), \ldots, \mathbf{x}^m(\mu_m)\right] \tag{15}$$

where *i* = 1,...*m*. In determining accessible output sets, surfaces generated by singularities may intersect each other. Parts of a surface may be internal while other parts may be boundary to the wrist accessible output set. Intersecting curves between surfaces determine a different type of singularity, which divide the surface into a number of subsurfaces. The set of generalized coordinates resulting from this intersection are higher order singularities (the so-called bifurcation points of a cross section of the accessible output set). Pairs of surfaces are intersected such that

$$\mathbf{x}^i(\mu_i) - \mathbf{x}^j(\mu_j) = 0 \quad \text{for } i \neq j \tag{16}$$

Eq. (16) will result in a number of higher order singularities. The number of singularities is augmented to μ_i, $i = 1, \ldots, m, m+1, \ldots, n$; where (*n*-*m*) is the number of surface intersections resulting in new singularities. The matrix of subsurfaces is augmented to

$$\Psi^i(\mu_\iota) = \left[\Psi^1(\mu_1), \Psi^2(\mu_2), \ldots, \Psi^m(\mu_m), \Psi^m(\mu_{m+1}), \ldots, \Psi^n(\mu_n)\right] \tag{17}$$

Equation (17) includes all subsurfaces due to internal, boundary, and higher order singularities. It remains to determine whether these subsurfaces are internal or boundary surfaces. This can be performed by *perturbing* a known point on the subsurface and determining whether this point satisfies the equation of constraint (Eq. 8), subject to inequality constraints of Eq. (9). For a subsurface $\Psi^i(\mathbf{q})$ due to a singularity μ_i, the normal to the surface at a known point $\mathbf{q}^o$, where q_1 and q_2 are generalized coordinates, is given as (Docarmo 1976)

$$\hat{\mathbf{n}}(\mathbf{q}^o) = \frac{\left(\dfrac{\partial \Psi^i}{\partial q_1} \times \dfrac{\partial \Psi^i}{\partial q_2}\right)}{\left|\dfrac{\partial \Psi^i}{\partial q_1} \times \dfrac{\partial \Psi^i}{\partial q_2}\right|} \tag{18}$$

For a small perturbation ∂t about the point $\mathbf{q}^o$ on the subsurface $\Psi^i(\mathbf{q})$ along the normal $\hat{\mathbf{n}}(\mathbf{q}^o)$, the coordinates of the perturbed points are

$$\mathbf{x} = \Psi^i(\mathbf{q}^o) \pm \partial t \hat{\mathbf{n}}(\mathbf{q}^o) \tag{19}$$

For the perturbed point to exist inside the accessible output set, it has to satisfy Eq. (8), subject to inequality constraints of Eq. (9). A solution is sought to the following system of equations.

$${}^0\mathbf{R}_3 \, {}^3\mathbf{x}_w + {}^0\mathbf{p}_3 - \Psi^i(\mathbf{q}^o) \mp \partial t \hat{\mathbf{n}}(\mathbf{q}^o) = \mathbf{0} \tag{20}$$

$$q_1^{\min} \leq q_1 \leq q_1^{\max} \tag{21a}$$

$$q_2^{\min} \le q_2 \le q_2^{\max} \tag{21b}$$

$$q_3^{\min} \le q_3 \le q_3^{\max} \tag{21c}$$

The subsurface $\Psi^i(\mathbf{q})$ *is an internal surface if and only if there exists a solution for Eq. (20) for both perturbations* $\pm\partial t$ *, consistent with the inequalities of Eq. (21).*

3. DETERMINING SERVICE REGIONS

To determine service regions at an operating point **p**, a service sphere parametrized as $\mathbf{x}_{ss}(s,t)$, is located with center at **p** and radius h (distance between point **p** on the end-effector and the wrist point ***W***). The wrist point assumes a position on the surface of the service sphere and has to satisfy Eq. (8). Using this definition, *the service region is defined as the points on the surfaces of the service sphere and inside the wrist accessible output set*. The service region $SR_i(\mathbf{p},\mathbf{q})$ is a set that exists on the surface of the service sphere

$$SR_i(\mathbf{p},\mathbf{q}) = \{\mathbf{x}_{ss}(\mathbf{p}) = \mathbf{0}, \textit{ for some } \mathbf{q}\} \tag{22}$$

and belongs to the wrist accessible output set such that

$$SR_i(\mathbf{p},\mathbf{q}) = \{\Phi(\mathbf{q}) = \mathbf{0}, \textit{ for some } \mathbf{q}\} \tag{23}$$

Since the boundary of the wrist accessible output set has been determined, it is possible to intersect each subsurface with the service sphere to determine the intersection curve. To determine whether the service region is enclosed by the intersecting curve, a ray is cast in the direction of the normal passing through ***p***. The ray will intersect the sphere in two points $\mathbf{s}_1$ and $\mathbf{s}_2$. The service region is identified by determining which of these points satisfies the local constraint equation. The *local constraint equation accounts* for the inequality constraint associated with the singularity of the subsurface. The intersection curve is the set of solutions to Λ_1 such that

$$\Lambda_1 = \begin{bmatrix} \Psi^i(\mathbf{q}) - \mathbf{x}_{ss}(s,t) \\ q_i - a_i - b_i \sin\lambda_i \end{bmatrix} = \mathbf{0} \tag{24}$$

The service region is identified by determining one of the points on the ray satisfying the following

$$\Lambda_2 = \begin{bmatrix} \Psi^i(\mathbf{q}) + t\hat{\mathbf{n}}(\mathbf{p}) - \mathbf{x}_{ss}(\mathbf{p}) \\ q^{local} - a - b\sin\lambda \end{bmatrix} = \mathbf{0} \tag{25}$$

Numerical solutions using the Newton-Raphson iteration method are obtained. To visualize service regions, it is convenient to introduce **dexterity charts**. Dexterity charts are projections of service regions onto another space. The intersection curve of each subsurface with the service sphere is parametrized in terms of parameters *s* and *t* on the surface of the sphere. Using a projection method (Taylor and Mann 1972), the curve is then mapped onto a cylinder and the cylinder is unrolled. The sphere $\mathbf{x}_{ss}(s,t)$ (with radius *h*) is mapped onto the cylinder $\mathbf{x}_c(u,v)$ (with radius *h*) such that the arc length in the uv-plane is given by

$$d\sigma^2 = du^2 + dv^2 = h^2dt^2 + dz^2 = h^2dt^2 + \left(\frac{dz}{d\beta}\right)^2 d\beta^2 \tag{26}$$

where θ is the longitude angle and β is the latitude angle. The arc length on the sphere is given by

$$d\sigma = h^2\cos^2\beta dt^2 + h^2 d\beta^2 \tag{27}$$

Dividing Eq. (26) by Eq. (27) and integrating using the requirement that $z = 0$ when $\beta = 0$ and $z > 0$ when $\beta > 0$ and substituting β with $(\pi/2 - s)$, the operator *L* is introduced such that

$$L[\mathbf{x}_{ss}(s,t)] = \mathbf{x}_c(u,v) \tag{28}$$

where the operator L is defined as follows.

$$L\begin{Bmatrix} s \\ t \end{Bmatrix} = \begin{Bmatrix} h\log\left(\sec(\frac{\pi}{2}-s)+\tan(\frac{\pi}{2}-s)\right) \\ ht \end{Bmatrix} = \begin{Bmatrix} u \\ v \end{Bmatrix} \tag{29}$$

4. ILLUSTRATING DETERMINATION OF THE WRIST BOUNDARY

To illustrate the foregoing analysis, consider the manipulator depicted in Fig. 2. The first segment of the manipulator comprises one prismatic and two revolute joints (Fig. 2a).

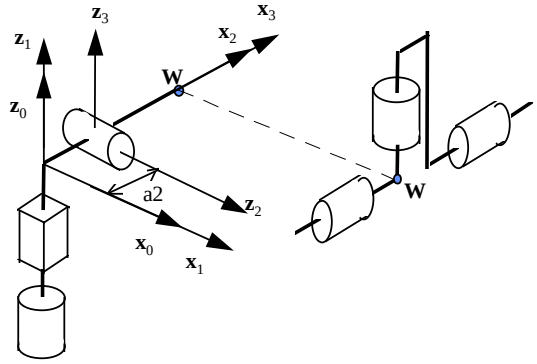

(a) (b)

Figure 2 (a) Three joints of a manipulator, (b) A spherical wrist (three intersecting axes)

For this manipulator, the three homogeneous transformation matrices (joints 1, 2, and 3) are

$$ {}^0\mathbf{T}_1 = \begin{bmatrix} 1 & 0 & 0 & 0 \\ 0 & 1 & 0 & 0 \\ 0 & 0 & 1 & q_1 \\ 0 & 0 & 0 & 1 \end{bmatrix} {}^1\mathbf{T}_2 = \begin{bmatrix} \cos q_2 & 0 & \sin q_2 & 0 \\ \sin q_2 & 0 & -\cos q_2 & a_2 \sin q_2 \\ 0 & -1 & 0 & 0 \\ 0 & 0 & 0 & 1 \end{bmatrix} \tag{30}$$

$$ {}^2\mathbf{T}_3 = \begin{bmatrix} \cos q_3 & 0 & -\sin q_3 & 0 \\ \sin q_3 & 0 & \cos q_3 & 0 \\ 0 & -1 & 0 & 0 \\ 0 & 0 & 0 & 1 \end{bmatrix} $$

where $q_1, q_2,$ and q_3 are the generalized variables representing joint angles. Multiplying $\prod_{i=1}^{3} {}^i\mathbf{T}_{i-1}$, and extracting the rotation matrix (Eq. 7)

$$ {}^0\mathbf{R}_3 = \begin{bmatrix} \cos q_2 \cos q_3 & -\sin q_2 & -\cos q_2 \sin q_3 \\ \sin q_2 \cos q_3 & \cos q_2 & -\sin q_2 \sin q_3 \\ \sin q_3 & 0 & \cos q_3 \end{bmatrix} \tag{31}$$

The position vector is

$$ {}^0\mathbf{p}_3 = \begin{bmatrix} a_2 \cos q_2 & a_2 \sin q_2 & q_1 \end{bmatrix}^T \tag{32}$$

For a wrist point located at ${}^3\mathbf{x}_w = \begin{bmatrix} 0 & 0 & d_w \end{bmatrix}^T$, where d_w is the distance along the z-axis of the wrist point with respect to reference frame 3, the equation of constraint (Eq. 8) of the wrist point is

$$\Phi(\mathbf{q}) = \begin{bmatrix} x - d_w \cos q_2 \cos q_3 - a_2 \cos q_2 \\ y - d_w \sin q_2 \cos q_3 - \sin q_2 a_2 \\ z - d_w \sin q_3 - q_1 \end{bmatrix} = \mathbf{0} \tag{33}$$

For the remainder of this discussion let $a_2 = 10$ and $d_w = 5$. This manipulator has joint constraints as follows

$$0 \le q_1 \le 20 \;\Rightarrow\; \mathrm{q}_1 = c_1 + c_2 \sin\lambda_1 \tag{34}$$

$$0 \le q_2 \le 270^o \;\Rightarrow\; \mathrm{q}_2 = b_1 + b_2 \sin\lambda_2 \tag{35}$$

$$-60^o \le q_3 \le 120^o \;\Rightarrow\; \mathrm{q}_3 = d_1 + d_2 \sin\lambda_3 \tag{36}$$

Where the generalized coordinates λ_i were introduced according to Eq. (13). Evaluating Eq. (14b)

$$\Phi_\lambda = \begin{bmatrix} 0 & -\sin(b_1 + b_2 \sin\lambda_2 b_2 \cos\lambda_2 \cos(d_1 + d_2 \sin\lambda_3) d_w - a_2 \sin(b_1 + b_2 \sin\lambda_2) b_2 \cos\lambda_2 \\ 0 & \cos(b_1 + b_2 \sin\lambda_2 b_2 \cos\lambda_2 \cos(d_1 + d_2 \sin\lambda_3) d_w - a_2 \cos(b_1 + b_2 \sin\lambda_2) b_2 \cos\lambda_2 \\ c_2 \cos\lambda_1 & 0 \end{bmatrix}$$

$$\begin{bmatrix} -\cos(b_1 + b_2 \sin\lambda_2) \sin(d_1 + d_2 \sin\lambda_3) d_2 \cos\lambda_3 d_w \\ \sin(b_1 + b_2 \sin\lambda_2) \sin(d_1 + d_2 \sin\lambda_3) d_2 \cos\lambda_3 d_w \\ \cos(d_1 + d_2 \sin\lambda_3) d_2 \cos\lambda_3 d_w \end{bmatrix} \tag{37}$$

Internal and boundary sigularities are computed by evaluating the determinant of the Jacobian and equating to zero

$$\left|\Phi_\lambda\right| = c_2 \cos\lambda_1 \sin(d_1 + d_2 \sin\lambda_3) d_2 \cos\lambda_3 d_w b_2 \cos\lambda_2 \left(\cos(d_1 + d_2 \sin\lambda_3) d_w + a_2\right) = 0 \tag{38}$$

subject to constraint Eq. (9). Singularities are determined by analyzing Eq. (38), as follows.

The first term of Eq. (38), $\cos\lambda_1 = 0$, indicates that $\lambda_1 = \frac{\pi}{2}, -\frac{\pi}{2}$. Substituting into Eq. (34) results in two singularities $q_1 = 0,\ 20$. For $\sin(d_1 + d_2 \sin\lambda_3) = 0$, $\sin(q_3) = 0$, i.e., two singularities $q_3 = 0,\ \pi$. For $\cos\lambda_3 = 0$, $\lambda_3 = \frac{\pi}{2}, -\frac{\pi}{2}$, i.e., two additional singularities $q_3 = -60^o,\ 120^o$. For $\cos\lambda_2 = 0$ $\lambda_2 = \frac{\pi}{2}, -\frac{\pi}{2}$, i.e., two singularities $q_2 = 0,\ 270^o$. Finally for $\cos(d_1 + d_2 \sin\lambda_3) d_w + a_2 = 0$, $\cos q_3 = -\frac{a_2}{d_w}$ will exist if and only if $a_2 < d_w$..

Note that only singularities that are consistent with the constraints are taken. The singularity $q_3 = \pi$ is *not consistent with the constraints* (does not satisfy Eq. (36)) thus it is not considered. The total number of singularities is 7. Surfaces are parametrized by substituting each singularity into Eq. (33). For example, the surface $\mathbf{x}^2$ due to singularity $q_1 = 20$ is readily determined.

$$\mathbf{x}^2(q_1 = 20) = \begin{bmatrix} \cos q_2 [-0.5 d_w + a_2] \\ \sin q_2 [-0.5 d_w + a_2] \\ 0.866 d_w + q_1 \end{bmatrix}, 0 \le q_2 \le 270^o \quad , \quad -60^o \le q_3 \le 120^o \tag{39}$$

and similarly,

$$\mathbf{x}^4(q_3 = -60) = \begin{bmatrix} \cos q_2[0.5d_w + a_2] \\ \sin q_2[0.5d_w + a_2] \\ -0.866d_w + q_1 \end{bmatrix} \text{where, } 0 \le q_2 \le 270^o \quad \text{and } 0 \le q_1 \le 20'' \tag{40}$$

and for surface $\mathbf{x}^5$, the parametrized surface is

$$\mathbf{x}^5(q_1 = 0) = \begin{bmatrix} \cos q_2[\cos q_3 d_w + a_2] \\ \sin q_2[\cos q_3 d_w + a_2] \\ \sin q_3 d_w \end{bmatrix} 0 \le q_2 \le 270^o \quad , -60^o \le q_3 \le 120^o \tag{41}$$

Figure 3a depicts each surface generated by the set of singularities. The union of these surfaces envelops the accessible set also shown in Fig 3a. Figure 3b is a cross section of the surfaces.

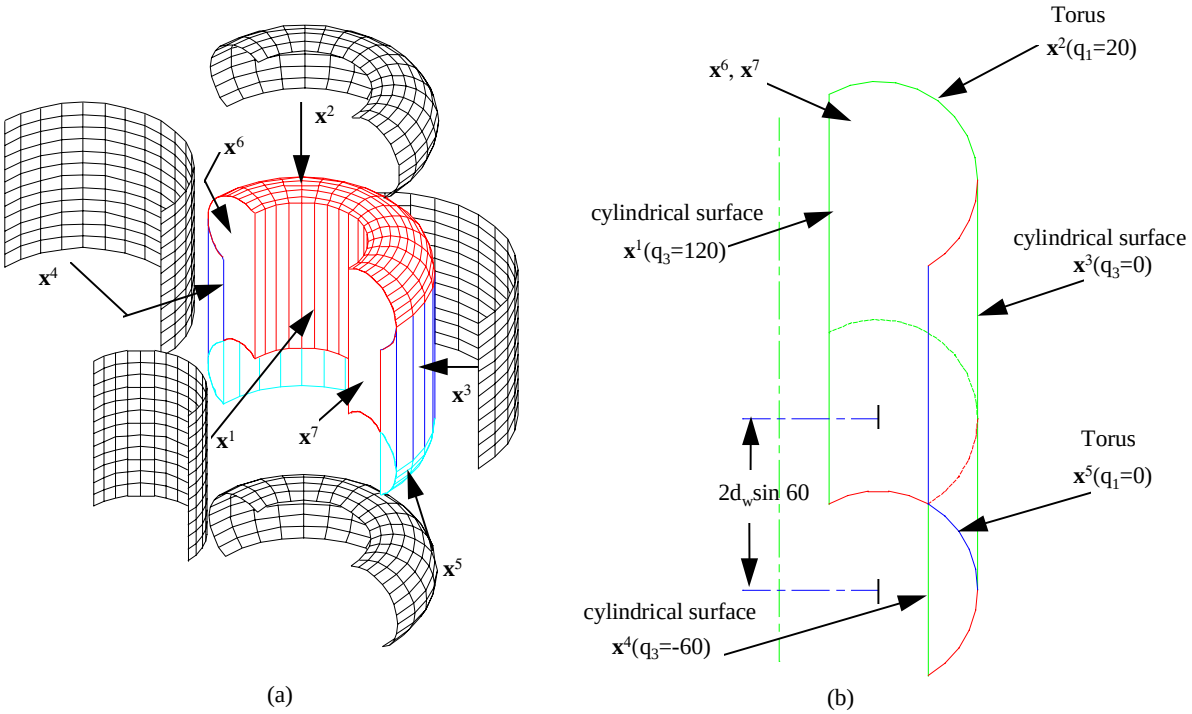

Figure 3 (a) A section of the wrist accessible output set
(b) A cross section of the wrist accessible output set

Note that surfaces $\mathbf{x}^6(q_2 = 0)$ and $\mathbf{x}^7(q_2 = 270^o)$ are planar surfaces. To illustrate the intersection of surfaces to determine higher order singularities, consider the intersection between the cylindrical surface $\mathbf{x}^4(q_3 = -60^o)$ and the torus $\mathbf{x}^5(q_1 = 0)$. The intersection curve between the two surfaces can be computed by solving the equation

$$\mathbf{x}^4 - \mathbf{x}^5 = \mathbf{0} \tag{42}$$

carrying out the algebra,

$$\cos q_3 = 0.5 \tag{43}$$

for $q_3 = -60^o$, and $q_1 = 0$, the curve is a circle with coordinates

$$\begin{bmatrix} (0.5d_w + a_2)\cos q_2 \\ (0.5d_w + a_2)\sin q_2 \\ 0 \end{bmatrix} \text{where } 0 \le q_2 \le 270^o \tag{44}$$

Similarly, the second curve where $q_3 = 60^o$, and $q_1 = 2d_w \sin 60^o$, the curve is a circle

$$\begin{bmatrix} (0.5d_w + a_2)\cos q_2 \\ (0.5d_w + a_2)\sin q_2 \\ 2d_w \sin 60^o \end{bmatrix} \text{where } 0 \le q_2 \le 270^o \qquad (45)$$

The first set ($q_3 = -60^o$, and $q_1 = 0$) are singularities similar to those resulting from Eq. (27). The second set ($q_3 = 60^o$, and $q_1 = 2d_w \sin 60^o$) is a higher order singularity set that has the effect of subdividing the surfaces into subsurfaces Ψ^i. Figure 4 depicts $\mathbf{x}^4$ having two subsurfaces: Ψ^3 (shown dotted) and Ψ^4 (shown solid). This means that $\mathbf{x}^4$ is segmented to subsurface Ψ^3 on the interval $q_1 \in [2d_w \sin 60 \quad 20]$, and subsurface Ψ^4 on the interval $q_1 \in [0 \quad 2d_w \sin 60]$.

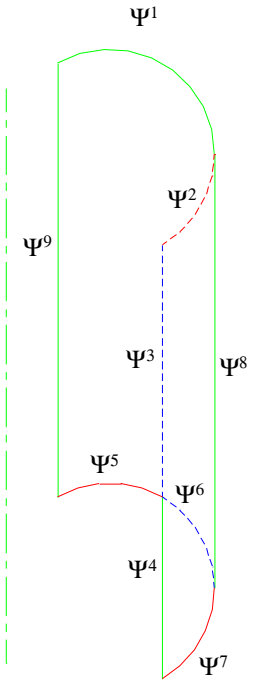

Figure 4 A cross-section of subsurfaces of the wrist accessible output set

Using this method of intersecting surfaces to find higher order singularities, the 7 surfaces are divided into 11 subsurfaces depicted in Fig. 4. Similarly, $\mathbf{x}^2$ has two subsurfaces: Ψ^2 on the interval $q_3 \in [-60 \quad 0]$, and Ψ^1 on the interval $q_3 \in [0 \quad 120]$. Surface $\mathbf{x}^5$ has three subsurfaces: Ψ^5 on the interval $q_3 \in [60 \quad 120]$, Ψ^6 on the interval $q_3 \in [0 \quad 60]$, and Ψ^7 on the interval $q_3 \in [-60 \quad 0]$, while the remainder of the surfaces are not subdivided (e.g., $\Psi^8 = \mathbf{x}^3$, $\Psi^9 = \mathbf{x}^1$).

To determine whether each subsurface is a boundary or internal subsurface to the wrist accessible output set, the perturbation method (Eq. 20) is performed. For example, consider a point on Ψ^1 in the mid range of its interval such that $q_2^o = \left(q_2^{\max} + q_2^{\min}\right)/2 = (0+270)/2 = 135^o$, $q_3^o = \left(q_3^{\max} + q_3^{\min}\right)/2 = (0+120)/2 = 60^o$, and the

third component is the singularity at $q_1^o = 20$. Thus the point on the surface is

$$\mathbf{q}^o = \begin{bmatrix} 20 & 135 & 60 \end{bmatrix}^T$$

The unit normal to Ψ^1 using Eq. (18) is

$$\hat{\mathbf{n}} = \begin{bmatrix} \cos q_2 (\cos q_3)^2 d_w^2 + \cos q_2 \cos q_3 d_w a_2 \\ \sin q_2 (\cos q_3)^2 d_w^2 + \sin q_2 \cos q_3 d_w a_2 \\ \sin q_3 \cos q_3 d_w^2 + \sin q_3 d_w a_2 \end{bmatrix} \tag{46}$$

The unit normal at the point $\mathbf{q}^o$ on the subsurface Ψ^1 is evaluated $\hat{\mathbf{n}}(\mathbf{q}^o) = \begin{bmatrix} -0.354 & 0.354 & 0.866 \end{bmatrix}^T$

Using Eq. (20), the subsurface Ψ^1 is an internal surface if and only if both perturbations $(\partial t = \pm 0.1)$ of $\mathbf{q}^o$ have solutions of the augmented matrix of Eq. (20) and Eq. (21). That is

$$\begin{bmatrix} \cos q_2 (\cos q_3 d_w + a_2) - \Psi_x^1(\mathbf{q}^o) - \partial t \hat{n}_x \\ \sin q_2 (\cos q_3 d_w + a_2) - \Psi_y^1(\mathbf{q}^o) - \partial t \hat{n}_y \\ \sin q_3 d_w + q_1 - \Psi_z^1(\mathbf{q}^o) - \partial t \hat{n}_z \\ q_1 - 10 - 10 \sin \lambda_1 \\ q_2 - \frac{3\pi}{4} - \frac{3\pi}{4} \sin \lambda_2 \\ q_3 - \frac{\pi}{6} - \frac{\pi}{2} \sin \lambda_3 \end{bmatrix} = 0 \tag{47}$$

For $\partial t = -0.1$ there exists a solution to Eq. (47) such that $\mathbf{q} = \begin{bmatrix} 19.98 & 135 & 60.06 \end{bmatrix}^T$. While for $\partial t = +0.1$ no solution can be found. Thus Ψ^1 is a boundary surface of the wrist accessible output set and is shown in Fig. 5b.

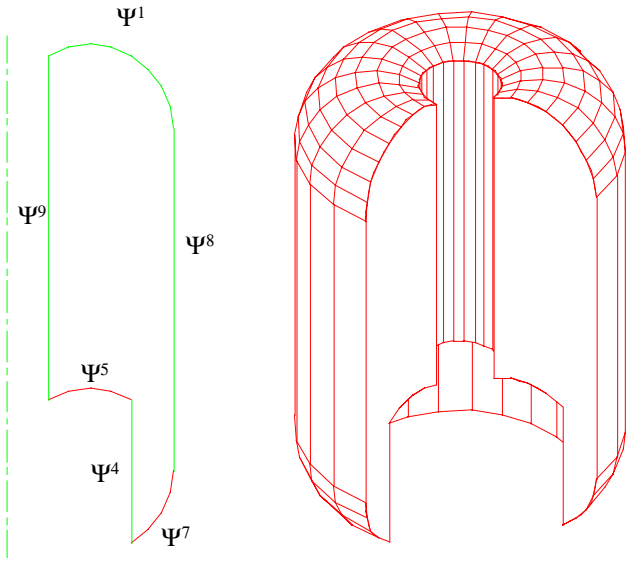

(a) (b)

Figure 5 (a) Boundary subsurfaces of the wrist accessible output set
(b) The wrist accessible output set

For subsurface Ψ^2, the point on the mid-range of the inequality constraints is $\mathbf{q}^o = [20 \quad 135 \quad -30]^T$. The normal to this surface at $\mathbf{q}^o$ is $\hat{\mathbf{n}}(\mathbf{q}^o) = [-0.612 \quad 0.612 \quad -0.5]^T$, and for ($\partial t = +0.1$) there exists a solution to Eq. (47) such that $\mathbf{q} = [19.98 \quad 135 \quad 60.06]^T$. Thus subsurface Ψ^2 is an internal subsurface. With knowledge of subsurfaces, the boundary of the wrist accessible output set is determined (depicted in Fig. 5b).

The above method was used to determine the accessible output set for a number of manipulator configurations. Figure 6a,b,c,d,e, and f depict accessible output sets for a variety of combination of revolute (R) and prismatic (P) joints.

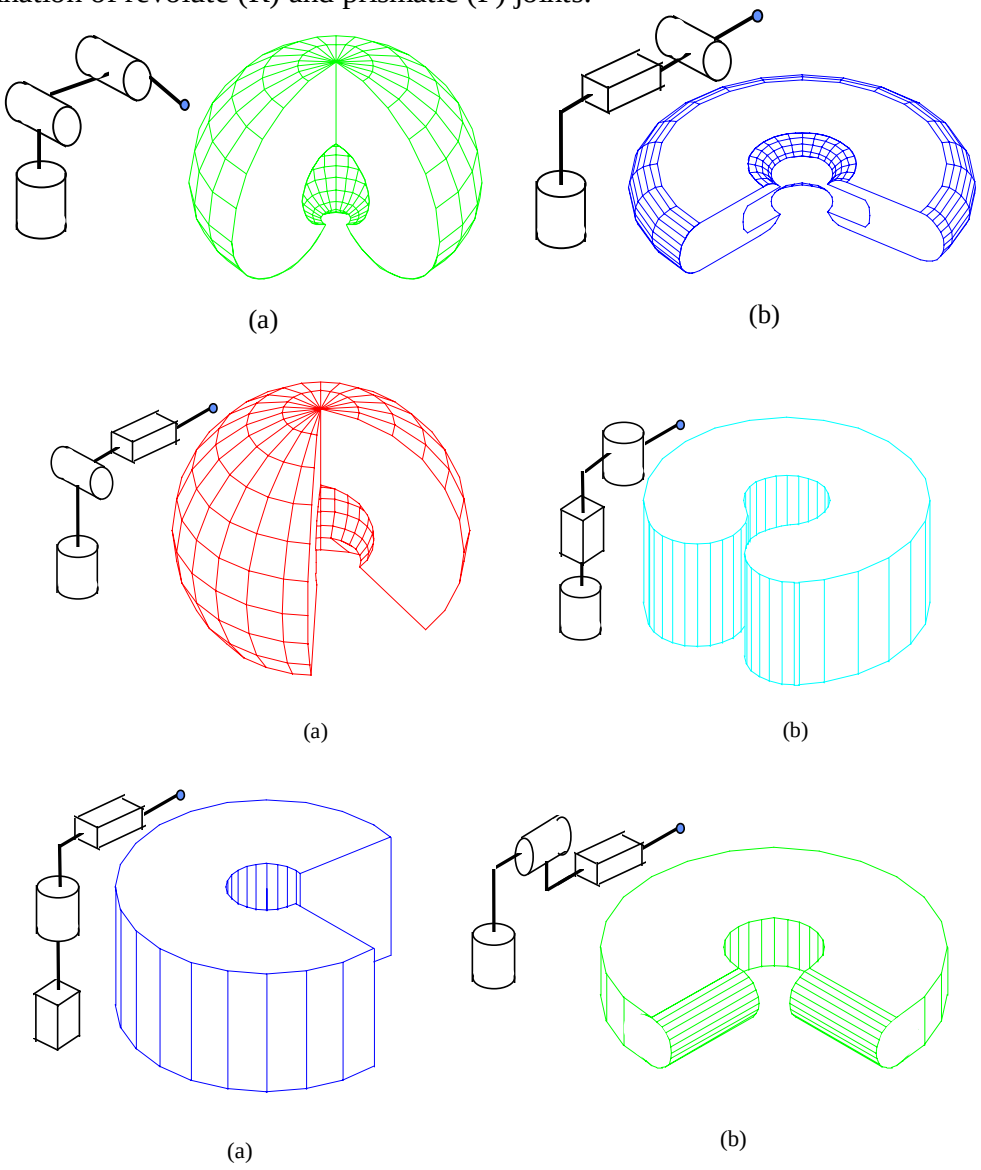

Figure 6 wrist accessible output set (a) RRR, (b) RPR, (c) RRP, (d) RPR, (e) PRP, and (f) RPR

5 ILLUSTRATING DETERMINATION OF SERVICE REGIONS

To illustrate the above formulation, consider the 6 DOF manipulator depicted in Fig. 7.

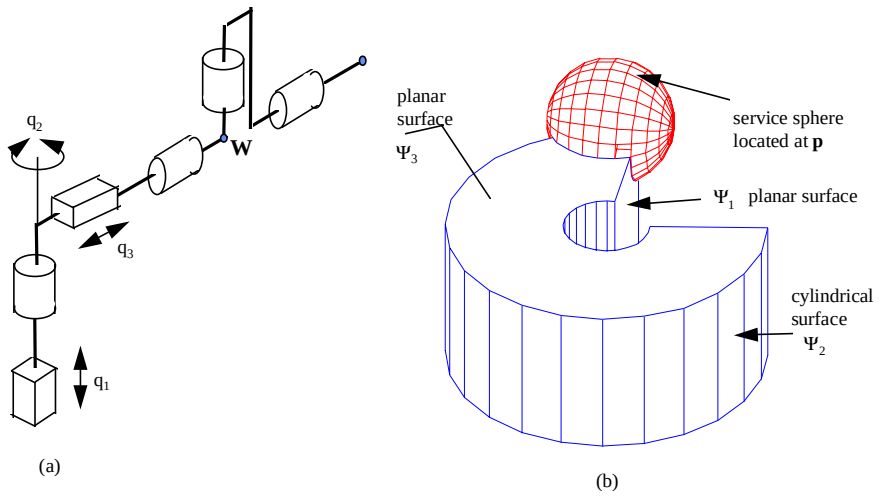

Figure 7 (a) kinematic skeleton of a six axis manipulator,
(b) service sphere located at a target **p** and intersecting the wrist accessible output set

The first three joints of the manipulator have inequality constraints

$$0 \le q_1 \le 10$$
$$-10^o \le q_2 \le 280^o$$
$$3 \le q_3 \le 10$$

The boundary of the wrist accessible output set of this manipulator has been studied and is depicted in Fig. 7b. At a point $\mathbf{p} = \begin{bmatrix} 11 & 0 & 10 \end{bmatrix}^T$ in the accessible output set, the service sphere is located. To determine the service regions of this manipulator, and hence the dexterity charts, the intersection between each subsurface and the service sphere is carried out. For example, consider the curve between subsurface Ψ^2 and the service sphere. The normal to Ψ^2 using Eq. (18) is calculated

$$\hat{\mathbf{n}} = \begin{bmatrix} \cos q_2 & \sin q_2 & 0 \end{bmatrix}^T \tag{48}$$

and Eq. (24) may be written as

$$\Lambda_1 = \begin{bmatrix} -10\sin q_2 - 11 - h\sin s\cos t \\ \cos q_2 - h\sin s\sin t \\ q_1 - 10 - \cos s \\ q_1 - 5 - 5\sin\lambda_1 \\ q_2 - \dfrac{3\pi}{4} - 2.53\pi\sin\lambda_2 \\ q_3 - 6.5 - 3.5\sin\lambda_3 \end{bmatrix} = 0 \tag{49}$$

Solving the above augmented matrix and projecting the solution onto the uv-plane using Eq. (28), it is now possible to visualize the boundary of the service region as depicted in Fig. 8.

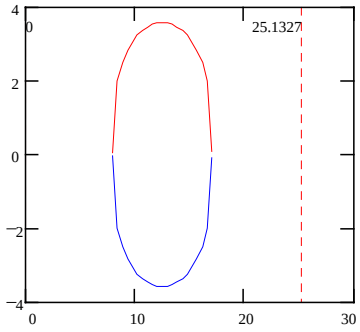

Figure 8 Boundary of a region due to subsurface Ψ^2

To determine whether the service region is enclosed by the boundary, the augmented matrix Λ_2 is solved such that

$$\Lambda_2 = \begin{bmatrix} h\sin s\cos t - w\cos q_2 \\ h\sin s\sin t - w\sin q_2 \\ h\cos t \\ q_3 - 6.5 - 3.5\sin\lambda_3 \end{bmatrix} = 0 \qquad (50)$$

The solution to Λ_2 results in two points $\mathbf{s}_1$ and $\mathbf{s}_2$. The solution to $\mathbf{x}_q(\mathbf{q}) - \mathbf{s}_1 = \mathbf{0}$ and $\mathbf{x}_q(\mathbf{q}) - \mathbf{s}_2 = \mathbf{0}$ is computed to determine the generalized coordinates $\mathbf{q} = \begin{bmatrix} 7 & 0 & 10 \end{bmatrix}^T$ and $\mathbf{q} = \begin{bmatrix} 15 & 0 & 10 \end{bmatrix}^T$ respectively. Only $\mathbf{s}_1$ satisfies the local constraint. In addition, $\mathbf{s}_1$ projected onto the uv-plane exists inside the intersection curve, which indicates that the region due to Ψ^2 is the shaded region depicted in Fig. 9.

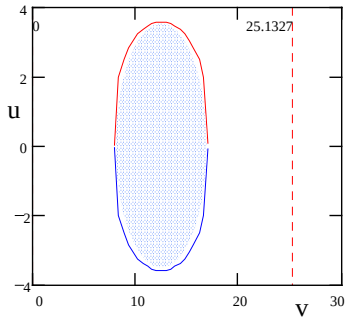

Figure 9 Service region due to subsurface Ψ^2

Similarly, the procedure is repeated for all subsurfaces intersecting the service sphere. The projection of the intersection curve of Ψ^1 with the service sphere and its region are depicted in Fig. 10a. The projection of the intersection curve Ψ^3 and its region are depicted in Fig. 10b.

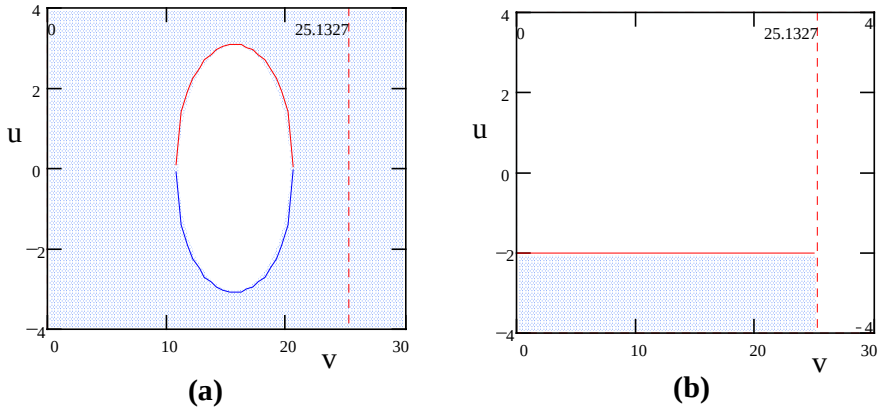

Figure 10 (a) Region due to subsurface Ψ^1, (b) Region due to subsurface Ψ^3

To determine the service region due to the wrist accessible output set, the regions are superimposed (Fig. 9, Fig. 10a, and Fig. 10b). The resultant service region is depicted in Fig. 11.

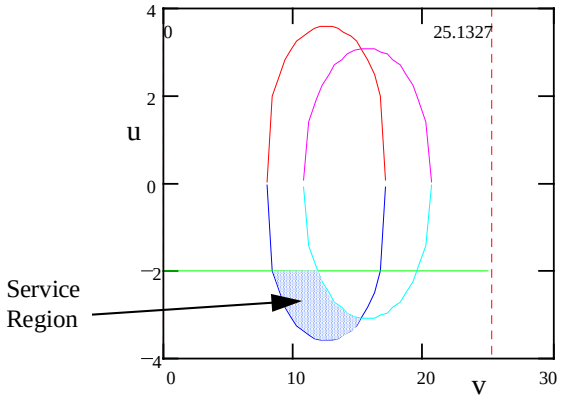

Figure 11 Service region at target **p** due to the wrist accessible output set

6 SERVICE REGIONS OF THE SPHERICAL JOINT

In order to complete the determination of dexterity charts, the service regions due to the joint limits of the spherical joint are computed. In order to motivate the discussion, consider a typical spherical wrist modeled as three revolute joints intersecting at a single point **W** (Pieper 1968). The point **p** may sweep regions on the surface of the sphere centered at **W**. Alternatively, we have defined the service sphere to be of radius *h* located at ***p***, thus the wrist point may assume location on regions on the service sphere. These regions are bound by arcs connecting the surface points $\mathbf{W}^j$. The coordinates of the wrist points $\mathbf{W}^j$ are determined by substituting maximum and minimum joint limits. At a target point ***p***, the mechanism is assembled and the constraint equation is

$$\mathbf{p} - {}^0\mathbf{R}_6\,{}^6\mathbf{x}_E - {}^0\mathbf{p}_6 = \mathbf{0} \tag{51}$$

where ${}^6\mathbf{x}_E$ is the vector describing a point on the end-effector with respect to link 6. The spherical wrist is constrained as

$$q_4^{\min} \le q_4 \le q_4^{\max} \tag{52a}$$

$$q_5^{\min} \le q_5 \le q_5^{\max} \tag{52b}$$

$$q_6^{\min} \le q_6 \le q_6^{\max} \tag{52c}$$

At a target point ***p***, and at any combination of the above joint limits, the coordinates of the wrist point is well defined for eight configurations (eight combinations of q_4, q_5, q_6). To compute the coordinates of the wrist point, the following equation is used.

$$\mathbf{W} = {}^0\mathbf{R}_4({}^4\mathbf{R}_6\,{}^6\mathbf{x}_E + {}^4\mathbf{p}_6) - \mathbf{p} \tag{53}$$

Each pair of wrist points is connected via an arc. To be able to project the arc connecting two wrist points $\mathbf{W}_1$ and $\mathbf{W}_2$ onto the uv-plane as well, a local coordinate system is formed at ***p*** with one of its axes along the vector from **p** to $\mathbf{W}_1$ such that

$$\mathbf{v}_1 = \mathbf{W}_1 - \mathbf{p} \tag{54}$$

and the perpendicular to the plane of the arc is

$$\mathbf{v}_3 = \mathbf{v}_1 \times (\mathbf{W}_2 - \mathbf{p}) \tag{55}$$

Finally the third orthogonal vector to both $\mathbf{v}_1$ and $\mathbf{v}_2$ is

$$\mathbf{v}_2 = \mathbf{v}_3 \times \mathbf{v}_1 \tag{56}$$

The rotation matrix relating the new coordinate system to the global reference frame is

$${}^0\mathbf{R}_B = \left[\mathbf{v}_1 \;\vdots\; \mathbf{v}_2 \;\vdots\; \mathbf{v}_3\right] \tag{57}$$

Wrist points on the arc can be generated along the arc such that

$${}^A\mathbf{W}_i = {}^0\mathbf{R}_B \begin{bmatrix} h\cos\beta_i \\ h\sin\beta_i \\ 0 \end{bmatrix} + \mathbf{p} \tag{58}$$

where the angle β_i is an incremental change such that $\beta_i = \beta_i + \Delta\left(Angle(\mathbf{v}_1, \mathbf{v}_2)\right)$. The boundary curve is then projected using the operator *L* (Eq. 29) such that

$$L\left({}^A\mathbf{W}_i(s,t)\right) = {}^A\mathbf{W}_i(u,v) \tag{59}$$

To illustrate, consider the spherical wrist of the PUMA arm with the following coordinate parameters.

Table 1 Denavit Harteneberg parameters of the PUMA arm

Joint i	θ_i	α_i	a_i	d_i	Joint limits
1	90	-90	0	0	
2	0	0	43	15	
3	90	90	-2	0	
4	0	-90	0	43	$-100^o \le q_4 \le 130^o$
5	0	90	0	0	$-100^o \le q_5 \le 100^o$
6	0	0	0	4	$-266^o \le q_6 \le 266^o$

It is required to determine the service region at a target point $\mathbf{p} = \left[65.458 \quad 49.015 \quad -19.942\right]^T$

The joint variables ($q_1, q_2,$ *and* q_3) are calculated using Eq. (51), and the corresponding wrist points (Eq. 53) are presented in table 2.

Table 2 Wrist points computed due to joint limits

Input q_4, q_5, q_6	q_1	q_2	q_3	Wrist point
$q_4 = 130^o, q_5 = -100^o$	30	23.5	67	$\mathbf{W}_1 = \left[63.9 \quad 54.215 \quad -15.52\right]^T$
$q_4 = 130^o, q_5 = +100^o$	22.46	30.65	65.41	$\mathbf{W}_2 = \left[68.16 \quad 44.42 \quad -24.47\right]^T$

$q_4 = -100^o, q_5 = -100^o$	21.37	30.45	58.11	$\mathbf{W'}_1 = \begin{bmatrix} 69.03 & 43.12 & -18.71 \end{bmatrix}^T$
$q_4 = -100^o, q_5 = +100^o$	31.06	23.03	75.61	$\mathbf{W'}_2 = \begin{bmatrix} 62.83 & 55.35 & -21.31 \end{bmatrix}^T$

A triad is created at ***p*** such that the rotation matrix (Eq. 57) is

$$ {}^0\mathbf{R}_B = \begin{bmatrix} 0.511 & 0.859 & 0.035 \\ -0.841 & 0.492 & 0.224 \\ 0.175 & -0.144 & 0.974 \end{bmatrix} $$

and the angle between $\mathbf{v}_1$ and $\mathbf{v}_2$ is computed ($Angle(\mathbf{v}_1, \mathbf{v}_2) = 171.29^o$). The arc is then projected onto the uv-plane using Eq. (59), where the service region is depicted in Fig. 12.

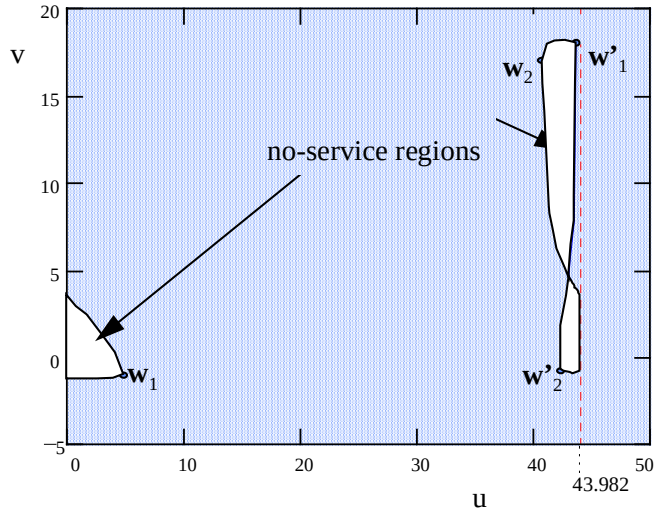

Figure 12 Service region due to the spherical joint

7. CONCLUSION

In this paper, a method for evaluating dexterity of robotic manipulators is presented. Using this analytic method, the kinematics of the manipulator are segmented into two parts. The wrist accessible output set is studied and analytically determined using the Jacobian of the manipulator. Singularities are computed and substituted into the constraint equation to parametrize surfaces. A difficulty was encountered in computing higher order singularities. Often times the computer program could not compute all singularities. The difficulty is currently being addressed.

At an operating point in the workspace, the service sphere is used to define service regions. The intersection curves resulting from the intersection of the boundary surfaces of the wrist accessible output set and the service sphere are projected onto dexterity charts. Dexterity charts are introduced in this paper to aid in visualizing manipulator orientability.

Service regions due to a spherical wrist are also determined by projecting the arcs connecting the wrist points due to spherical joint limits. Projecting the service regions onto dexterity charts provide a complete description of the functionality of a manipulator at a target.

8. REFERENCES

Abdel-Malek, K., 1993, *Off-Line Programming Using Commercial CAD Systems, and Design Criteria for Inherently High Accuracy Robots*, Ph.D. Dissertation, University of Pennsylvania, Philadelphia, PA.

Abdel-Malek, K., Paul, B., 1994, "The Dexterous Solid Angle for Manipulators with a Spherical Wrist," *Proceedings of the 23rd ASME Mechanisms Conference*, Minneapolis, MN.

Docarmo, M., 1976, *Differential Geometry of Curves and Surfaces*, Prentice Hall, Eenglewood Cliffs, NJ.

Denavit, J., and Hartenberg, R.S., 1955, "A Kinematic Notation for Lower-Pair Mechanisms Based on Matrices," *Journal of Applied Mechanics, ASME*, vol. 22, pp. 215-221.

Emiris, D.M., 1993, Workspace Analysis of Realistic Elbow and Dual-Elbow Robot," *Mechanisms and Machine Theory*, v.28, n.3, pp.375-396.

Flanders, H., Korfhage, R.R., and Price, J.J., 1970, *Calculus*. Academic Press, Inc. New York.

Gosselin, C, and Angeles, J., 1990, Singularity Analysis of Closed Loop Kinematic Chains," *IEEE Trans. on Robotics and Automation*, v.6, n.3, pp. 281-290.

Haug, E.J., et al., 1994, "Numerical Algorithms for Mapping Boundaries of Manipulator Workspaces," *Proceedings of the 23rd ASME Mechanisms Conference*, Minneapolis, MN.

Hilderbrand, F.B., 1976, *Advanced Calculus for Applications*. 2nd ed., Prentice-Hall, Inc., Englewood Cliffs, N.J.

Kumar, V., 1985, *Robot Manipulators-Workspaces and Geometric Dexterity*, Masters Thesis, The Ohio State University

Kumar, A., and Waldron, K.J., 1980, "The Dextrous Workspace," ASME Paper No. 80-DET.

Lai, Z.C. et. al., 1988, "The Dexterous Workspace of Simple Manipulators," *IEEE J. Robotics and Automation*, vol.4, No.1.

McKerrow, P.J., 1991, *Introduction to Robotics*, Addison Wesley.

Pieper, D.L., 1968, "The Kinematics of Manipulators Under Computer Control," Stanford Artificial Intelligence Laboratory, Stanford University, AIM 72.

Roth, B., 1975, "Performance Evaluation of Manipulators from a Kinematic Viewpoint," NBS Special Publications No.459, pp.39-61.

Rivin, E.I., 1988, *Mechanical Design of Robots*, McGraw-Hill, Inc., New York.

Taylor A.E. and Mann, W.R., 1972, *Advanced Calculus*, Xerox, Corp.

Tsai, Y.C., and Soni, A.H., 1981, "Accessible Region and Synthesis of Robot Arms," *J. of Mech. Design*, 103:803-811

Vinagradov, I., et.al., 1971, “Details of Kinematics of Manipulators with the Method of Volumes," (in Russian) *Mexanika Mashin*, No.27-28, pp.5-16.

Yang, D.C.H., and Lee, T.W., 1983, “On the Workspace of Mechanical Manipulators”, *J. of Mechanisms, Transmission and Automation Design*, 105:62-69.

Yang, D.C.H., et. al., 1985, "On the Dexterity of Robotic Manipulators-Service Angle," *Transactions of ASME, J.of Mech., Transm., and Automation in Design*, vol.107.

Wang, J.Y., and Wu, J.K., 1993, “Dexterous Workspaces of Manipulators, Part 2: Computational Methods,” *Mechanics of Structures and Machines*, 21(4):471-506.